The Astrophysical Journal, 621:875–883, 2005 March 10
© 2005. The American Astronomical Society. All rights reserved. Printed in U.S.A.

A GLOBAL TEST OF A QUASI-UNIVERSAL GAMMA-RAY BURST JET MODEL THROUGH MONTE CARLO SIMULATIONS

Xinyu Dai[1,2] and Bing Zhang[3]
Received 2004 July 13; accepted 2004 November 19

ABSTRACT

The possibility that long gamma-ray burst (GRB) jets are structured has received growing attention recently, and we have suggested that most GRBs and their softer, less energetic brethren, X-ray flashes (XRFs), can be understood within a quasi-universal structured jet picture, given that the jet structure of each individual burst is a Gaussian or similar function. Here we perform a global test on such a quasi-universal Gaussian-like structured jet by comparing Monte Carlo simulation results with a broad spectrum of observational data. Using the same set of input parameters as in previous work by Zhang and coworkers, we confront the model with more observational constraints. These constraints include the burst redshift distribution, jet break angle distribution, two-dimensional redshift versus jet break angle distribution, luminosity function, and $\log N - \log P$ distribution. The results indicate that the model is generally compatible with the data. This conclusion, together with our previous tests with the observed jet break angle versus isotropic energy and observed peak energy versus fluence relations, suggests that current long GRB and XRF data are generally consistent with such a quasi-standard energy and quasi-standard angle jet picture. With future homogeneous burst samples (such as the one to be retrieved from the *Swift* mission), the refined GRB jet structure can be further constrained through a global comparison between various observed and predicted burst property distributions and relations.

Subject heading: gamma rays: bursts

1. INTRODUCTION

The geometrical configuration is an essential ingredient in characterizing and understanding astrophysical phenomena. There is growing evidence that long gamma-ray bursts (GRBs) originate from collimated jets. This has been mainly suggested by an achromatic steepening break observed in many GRB afterglow light curves (Rhoads 1999; Kulkarni et al. 1999; Harrison et al. 1999). This interpretation receives indirect support from the intriguing fact that the geometry-corrected total energy in the GRB fireball is essentially constant (Frail et al. 2001; Bloom et al. 2003), i.e., $E_{\rm jet} = E_{\rm iso}(1 - \cos\theta_j) \sim$ const, where $E_{\rm iso}$ is the total energy emitted in the gamma-ray band assuming isotropic emission, and θ_j is the jet angle inferred from the light-curve breaks. In view of these facts, there are two distinct approaches in constructing jet models. One is that different GRBs collimate the same total energy into different angular openings, with the angular energy distribution within the jet being constant (Rhoads 1999; Frail et al. 2001). Another is a family of quasi-universal structured jet models, where the structured jet has a power-law or a Gaussian (or functions in more general forms) angular energy distribution with respect to the jet axis (Zhang & Mészáros 2002a; Rossi et al. 2002; Lloyd-Ronning et al. 2004). In the former scenario, the jet opening angle exclusively defines the jet break angle θ_j, while in most cases in the later scenario, θ_j is interpreted as the observer's viewing angle. It is essential to understand whether the GRB jets are structured, and if yes, how they are structured. This has important implications for the fundamental questions such as the total energy budget in the explosion, the physical origin of the collimation, and the birth rate of the GRB progenitor.

In this paper we define a "structured jet" as a jet with a certain functional angular distribution structure of energy (and possibly Lorentz factor as well), such as the power-law function with various indices, the Gaussian function, or numerous other possible structures one can think of. Since it is directly connected to the $E_{\rm iso} \propto \theta_j^{-2}$ (Frail et al. 2001) correlation, one particular structured jet model, i.e., the power-law jets with index -2 (Rossi et al. 2002; Zhang & Mészáros 2002a), has received broad attention. We call this special type of jet the "universal jet" following the convention in the literature, since it has the potential to interpret all GRB data with a universal configuration. We note that in some papers, "universal jets" and "structured jets" have been used interchangeably, which, in our opinion, may cause confusion for the readers, since a certain criticism to the universal jet model may not apply to more general structured jet models with other jet structures. The conventional top-hat jets are called "uniform jets" in this paper.

The need to understand GRB jets is boosted by the recent identification of X-ray flashes (XRFs; Heise 2003; Kippen et al. 2003), a fainter and softer version of GRBs, as a closely related phenomenon with GRBs. Recent observations reveal another intriguing empirical correlation between the cosmic rest-frame GRB spectral peak energy and the isotropic gamma-ray energy, i.e., $E_{\rm peak} \propto (E_{\rm iso})^{1/2}$, which was identified in the *BeppoSAX* (Amati et al. 2002) or even BATSE (Lloyd et al. 2000) GRB data and was also found to extend to the XRF regime in the *HETE-2* data (Lamb et al. 2005; Sakamoto et al. 2004). Although obvious outliers (e.g., GRB 980425) exist, the correlation is found to be valid within the time-dependent spectra of individual BATSE bursts (Liang et al. 2004a). This result strengthens the empirical law, which suggests that it is related to some intrinsic physical processes. The relation is understandable within the currently leading GRB models if a certain

[1] Department of Astronomy, 4055 McPherson Laboratory, The Ohio State University, 140 West 18th Avenue, Columbus, OH 43210; xinyu@astronomy.ohio-state.edu.

[2] Department of Astronomy and Astrophysics, Pennsylvania State University, 525 Davey Laboratory, University Park, PA 16802; xdai@astro.psu.edu.

[3] Department of Physics, University of Nevada, 4505 Maryland Parkway, Box 4002, Las Vegas, NV 89154; bzhang@physics.unlv.edu.

correlation between the bulk Lorentz factor and the burst luminosity is assumed (Zhang & Mészáros 2002b), i.e., $\Gamma \propto L^k$ with k having different values for different models. In particular, it is consistent with the internal shock model if the bulk Lorentz factor (and hence the internal shock radius) is insensitive to the burst luminosity, i.e., $k = 0$. In this paper we assume that the $E_{\rm peak}$-$E_{\rm iso}$ correlation holds for the majority of GRBs and XRFs.

In addition, the *HETE-2* sample bursts also indicate another interesting fact that the contributions to the total number of bursts from GRBs, X-ray–rich GRBs (XRGRBs), and XRFs are approximately equal (Lamb et al. 2005). This fact presents an important criterion to test the validity of any jet model.

The similarities between GRBs and XRFs have stimulated studies toward unifying the GRB and XRF phenomena through different geometrical configurations (e.g., Lamb et al. 2005; Yamazaki et al. 2003; Zhang et al. 2004). Lamb et al. (2005) pointed out that the universal jet model is inconsistent with the GRB-XRGRB-XRF number ratios detected by *HETE-2* and suggested a uniform jet model for all GRBs and XRFs. If one assumes a standard energy budget for all GRBs and XRFs, such a uniform jet model unavoidably leads to the conclusion that GRBs have very narrow jets with typical opening angle smaller than 1°. The universal jet model was also recently tested against various criteria (e.g., Perna et al. 2003; Nakar et al. 2004; Guetta et al. 2005b), and it has been found that such a model may violate some observational constraints. However, a pure universal jet model corresponds to a strict $E_{\rm iso} \propto \theta_j^{-2}$ relation. In reality, the data indicate that this correlation is only valid in a statistical sense (Frail et al. 2001; Bloom et al. 2003). In the $E_{\rm iso}$-θ_j plane, the afterglow data are distributed around the $E_{\rm iso} \propto \theta_j^{-2}$ line with moderate scatter (Lloyd-Ronning et al. 2004). This fact alone already suggests that GRB jets are not "universal." Any jet model aiming to interpret the GRB phenomenology is at best "quasi-universal," i.e., different jets may share more or less the same structure, but the parameters to define the structure should have some scatter around some typical values. An important insight is that when parameter scatter is taken into account, the jet structure is no longer obliged to be a power law with a -2 index. Other jet structures are also allowed (Lloyd-Ronning et al. 2004). In particular, we (Zhang et al. 2004) recently proposed a quasi-universal model for GRBs and XRFs. In order to successfully reproduce the correct relative numbers of GRBs, XRGRBs, and XRFs, we suggest that the jet structure in individual bursts is Gaussian-like or with a similar structure. This *Ansatz* was verified with a Monte Carlo simulation, and the model can also reproduce the $E_{\rm iso}$-θ_j relation. Considering that the narrow uniform jet model (Lamb et al. 2005) conflicts with the standard afterglow model (Zhang et al. 2004) and that the universal jet model encounters various difficulties (e.g., Lamb et al. 2005; Guetta et al. 2005b), we tentatively suggest that the quasi-standard energy and quasi-standard angle Gaussian-like jet model is a more plausible one to interpret GRB and XRF data in a unified manner.

In order to prove this suggestion, the quasi-universal jet model needs to confront a broader spectrum of data. Since within a structured jet model the probability of observing the jet at angle θ_v is proportional to $\sin\theta_v$, many observational properties can be predicted once the jet structure function and the variation parameters are given. In this paper, besides the $E_{\rm peak}^{\rm obs}$ versus fluence relation and the $E_{\rm iso}$-θ_j relation we have already tested in Zhang et al. (2004), we consider several new constraints including the burst redshift (z) distribution, jet angle (θ_j) distribution, two-dimensional z-θ_j distribution, luminosity function, and $\log N - \log P$ distribution. Some of these criteria have been taken individually to test some jet models (e.g., Perna et al. 2003; Lloyd-Ronning et al. 2004; Lin et al. 2004; Liang et al. 2004b; Nakar et al. 2004; Guetta et al. 2005b). However, none of the previous studies performed a global test for a particular model with all the criteria. We believe that such a global test is essential to constrain and to finally pin down the correct GRB jet structure. Here we perform such a test with the quasi-universal Gaussian-like jet model (Zhang et al. 2004). The exact GRB structure may differ from the simple Gaussian form. We take this simple structure as the starting point to examine how well it could reproduce the data. Because of the quasi-universal nature, analytical studies may not be adequate, and we perform a set of Monte Carlo simulations to access the problem.

2. MONTE CARLO SIMULATIONS

We perform Monte Carlo simulations for a quasi-universal Gaussian-like jet model. The jet structure and the input parameters that we use are the same as those used in Zhang et al. (2004), where the motivation to introduce such a jet structure is also explained. Below we describe the parameters of this model in more detail.

First, we approximate the angular energy distribution of the jet as

$$\epsilon(\theta) = \epsilon_0 e^{-\theta^2/2\theta_0^2}. \tag{1}$$

The total energy of the jet, E_j, is obtained by integrating $\epsilon(\theta)$ over the entire solid angle

$$E_j = 4\pi \int_0^{\pi/2} \epsilon(\theta) \sin\theta \, d\theta. \tag{2}$$

With a small θ_0, the total jet energy is approximately $E_j \sim 2\pi\epsilon_0\theta_0^2$ (Zhang & Mészáros 2002a). This jet structure contains two parameters, the total energy of the jet, E_j, and the characteristic jet width, θ_0. The parameters, E_j and θ_0, are distributed in lognormal distributions for the simulated bursts. This quasi-universal approach is required to reproduce the large scatter of the $E_{\rm iso}$-θ_j relation of GRBs (Lloyd-Ronning et al. 2004). In particular, these two parameters are constrained to be around (Zhang et al. 2004)

$$\left\langle \log\left(\frac{E_j}{1\ {\rm erg}}\right)\right\rangle \sim 51.1, \tag{3}$$

$$\sigma_{\log[E_j/(1\ {\rm erg})]} \sim 0.3, \tag{4}$$

$$\left\langle \log\left(\frac{\theta_0}{1\ {\rm rad}}\right)\right\rangle \sim -1.0, \tag{5}$$

$$\sigma_{\log[\theta_0/(1\ {\rm rad})]} \sim 0.2. \tag{6}$$

Although the definition E_j in the Gaussian structured jet model (eq. [2]) is different from that in the uniform jet model, our best-fit typical jet energy (eq. [3]) is consistent with the one in the uniform jet model (Bloom et al. 2003). We have shown that this set of input parameters can roughly reproduce the approximately equal numbers of GRBs, XRGRBs, and XRFs, the $E_{\rm iso}$-θ_j relation, and the $E_{\rm peak}^{\rm obs}$-fluence relation.

Second, in a structured jet model the observing angle, θ_v, is distributed as

$$\frac{dN(\theta_v)}{d\theta_v} = \sin\theta_v. \tag{7}$$

The isotropic equivalent energy, $E_{\rm iso}$, is defined as

$$E_{\rm iso} = 4\pi\epsilon(\theta_v). \tag{8}$$

The jet break angle, θ_j, of a Gaussian jet is (Kumar & Granot 2003; Zhang et al. 2004; Rossi et al. 2004)

$$\theta_j = \begin{cases} \theta_0, & \theta_v < \theta_0, \\ \theta_v, & \theta_v \geq \theta_0. \end{cases} \tag{9}$$

Finally, the number of bursts per unit redshift, $N(z)$, is distributed as

$$\frac{dN(z)}{dz} = \frac{R_{\rm GRB}(z)}{1+z}\frac{dV(z)}{dz}, \tag{10}$$

where $dV(z)/dz$ is the comoving volume per unit redshift and $R_{\rm GRB}$ is the GRB rate. The comoving volume is obtained as

$$\frac{dV(z)}{dz} = \frac{4\pi D_L^2 c}{(1+z)^2 H_0}\left[\Omega_m(1+z)^3 + \Omega_k(1+z)^2 + \Omega_\Lambda\right]^{-1/2}, \tag{11}$$

where $H_0 = 70$ km s^{-1} Mpc^{-1}, $\Omega_m = 0.3$, $\Omega_k = 0$, $\Omega_\Lambda = 0.7$, and D_L is the luminosity distance. We assume that the GRB rate traces the star-forming rate such that

$$R_{\rm GRB}(z) = \begin{cases} R_0 10^{0.75z}, & z < z_{\rm peak}, \\ R_0 10^{0.75 z_{\rm peak}}, & z \geq z_{\rm peak}. \end{cases} \tag{12}$$

Here we used the Rowan-Robinson star-forming rate (Rowan-Robinson 1999; cf. Lin et al. 2004). Two sets of burst redshifts are simulated with the parameter $z_{\rm peak} = 2$ and $z_{\rm peak} = 1$.

We simulate 10,000 bursts. For each burst we simulate E_j, θ_0, θ_v, and z according to the distributions those parameters follow. We calculate other parameters of the simulated bursts in the following equations. The peak energy of the simulated bursts are calculated through the $E_{\rm iso}$-$E_{\rm peak}$ relation (Amati et al. 2002),

$$E_{\rm peak} \sim 100\ {\rm keV}\left(\frac{\rm E_{iso}}{10^{52}\ {\rm ergs}}\right)^{1/2}, \tag{13}$$

in which we introduced lognormal scatter (with $\sigma \sim 0.3$) to reflect the statistical nature of the observed data points. The observed peak energy is related to the rest-frame peak energy by

$$E_{\rm peak}^{\rm obs} = E_{\rm peak}/(1+z), \tag{14}$$

and the burst energy fluence is calculated as

$$F = \frac{E_{\rm iso}(1+z)}{4\pi D_L^2}. \tag{15}$$

In order to obtain the peak flux or peak luminosity of the bursts, we simulate the conversion timescale T in the rest frame of the bursts as a lognormal distribution (see also Lamb et al. 2005),

$$\left\langle \log\left(\frac{T}{1\ {\rm s}}\right)\right\rangle \sim 0.56, \tag{16}$$

$$\sigma_{\log[T/(1\ {\rm s})]} \sim 0.05, \tag{17}$$

such that

$$L_{\rm peak} = E_{\rm iso}/T, \tag{18}$$

$$f_{\rm peak} = \frac{F}{T(1+z)}. \tag{19}$$

The central value of this distribution, 3.63 s, is consistent with the value of 3.41 s obtained from the *HETE-2* and *BeppoSAX* burst sample (Lamb et al. 2005). We note that this conversion timescale should be shorter than the true duration of the burst, since the peak flux is higher than the average flux. The exact central value used in this paper is obtained as the best fit to the BATSE peak flux distribution through a series of simulations with different central values (see § 3.5).

The simulated bursts are filtered by different detection thresholds that represent the sensitivities of different surveys. In principle, the thresholds should be calculated in units of peak photon flux. The peak photon flux depends on the spectral shape of the bursts, and the sensitivity is also a function of photon energy. Moreover, most of the bursts observed are strongly variable. For simplicity, here we use the simulated burst fluence to define various detection thresholds in most of the simulations except for the $\log N - \log P$ distribution.

3. RESULTS

After obtaining the sample of the simulated bursts with various burst parameters calculated, we compare the simulation results with current observations and perform a global test to the GRB jet structure with the observational constraints. The constraints include the burst redshift distribution, jet break angle distribution, redshift versus jet break angle two-dimensional distribution, luminosity function, $\log N - \log P$ distribution, $E_{\rm iso}$-θ_j relation, $E_{\rm peak}^{\rm obs}$-fluence relation, and the relative numbers of GRBs, XRGRBs, and XRFs. We note that the last three tests have been presented in a previous paper (Zhang et al. 2004). Here we only present the rest of the simulation results.

3.1. *Redshift Distribution*

There are two major uncertainties for the simulated burst redshifts. First, we assume that the GRB rate traces the star-forming rate, which may involve some uncertainties. In addition, the underlying star-forming rate itself is not accurately constrained. The observed redshift distribution of the bursts can be used, as a first step, to constrain the star-forming rate used in the simulation. We note that the jet structure will also affect the shape of the redshift distribution because of the limited sensitivities of the detectors. A homogeneous sample would be most suitable for these studies. The current sample of the bursts with redshift measurements is, however, small and inhomogeneous. Nonetheless, we compare this sample with the simulation results to obtain some preliminary understanding of the issue.

We plot the redshift distributions of the simulated bursts and compare with the sample obtained from the observations (Fig. 1). Figures 1*a* and 1*b* represent simulations with two different star-forming rates, with $z_{\rm peak} = 2$ and $z_{\rm peak} = 1$, respectively. The observed burst redshifts are obtained from Bloom et al. (2003) and the GRB Localization Web site[4] maintained by J. Greiner, and there are 37 bursts with measured redshifts in total. We select the simulated bursts with different detecting thresholds. The thresholds are set to be 1.0×10^{-5} and 5×10^{-8} ergs cm^{-2}. The first threshold is selected to be much higher than the triggering thresholds for most detectors in order to reflect the selection effect that only a small number of bright GRBs have their redshifts measured. For example, the median fluence value of the 28 bursts with redshift measurements in

[4] The GRB Localization Web site is at http://www.mpe.mpg.de/~jcg/grbgen.html.

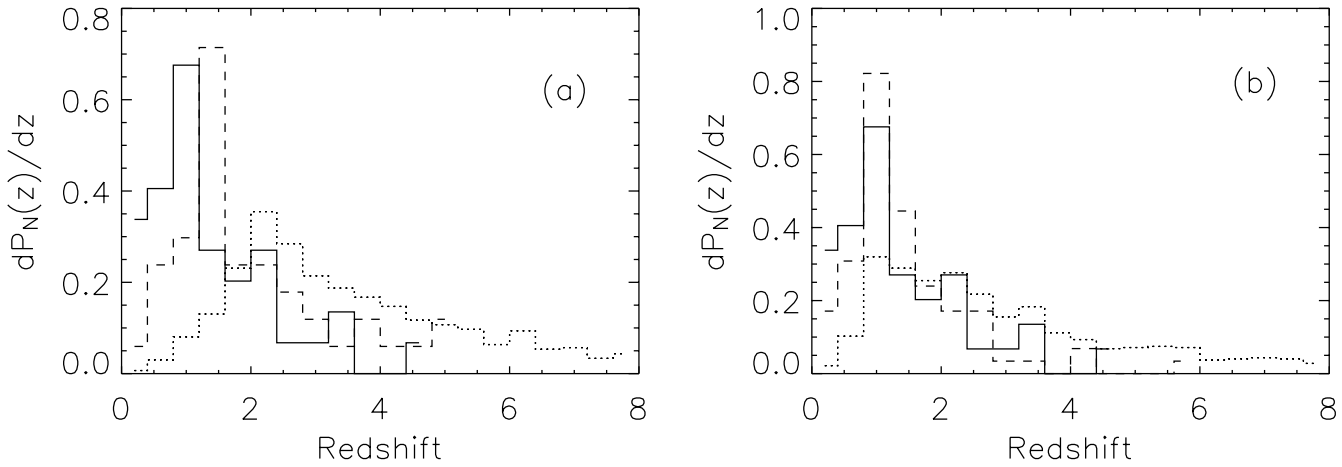

FIG. 1.—(*a*) Probability distribution functions of GRBs with respect to redshift for the observed bursts (*solid line*) and the simulated bursts with different detection thresholds for a $z_{\rm peak} = 2$ Rowan-Robinson star-forming rate. In particular, the dotted and dashed lines are simulated distributions with fluence thresholds of 5×10^{-8} and 1×10^{-5} ergs cm^{-2}, respectively. (*b*) Same as (*a*), but for $z_{\rm peak} = 1$.

Bloom et al. (2003) is 2.3×10^{-5} ergs cm^{-2}. The second threshold is selected to match the sensitivity of *HETE-2*.

Figure 1 shows that the observed redshift distribution peaks at $z \sim 1$. The observed distribution is consistent with both simulated distributions with different $z_{\rm peak}$, if a high detection threshold of 1.0×10^{-5} ergs cm^{-2} is adopted. This high threshold is reasonable to apply here when comparing the simulated redshift distribution with the currently observed redshift distribution, because only a few bursts have their redshifts measured. These bursts only account for a small fraction of the total amount of bursts detected, and they are typically brighter. In order to better illustrate this point, we show in Figure 2 the redshift versus fluence plots for the simulated bursts and the observed bursts from the Bloom et al. (2003) sample. Both star-forming rate models have been plotted. We can see that most of the observed bursts are concentrated in the high-fluence end compared with the simulated bursts. The current observed redshift sample cannot distinguish between the two star-forming rates. However, as a more homogeneous GRB redshift sample is accumulated (with future instruments such as *Swift*), the peak of the GRB rate can be constrained as the two models predict different peaks as the detection threshold decreases. We adopt $z_{\rm peak} = 2$ when discussing the simulation results below. An even larger and more homogeneous sample is needed in order to constrain the shape of the star-forming rate, especially whether the star forming rate is above or below the Rowan-Robinson rate at large redshifts ($z > 2$). For $z_{\rm peak} = 2$, the current data provide tentative evidence that the nearby events are more abundant than what is expected from the model that assumes the standard star-forming rate. For $z_{\rm peak} = 1$, the current model meets the data in the low-redshift regime as well. Whether extra nearby GRBs exist is of great interest in the GRB community, and more redshift data are needed before a firm conclusion is drawn.

We note that most XRFs do not have redshift measurements, which may present a bias in the observed sample. However, this should not affect the result too much, because the current redshift sample of GRBs is small (37 in total). Considering the number ratio of GRBs to XRFs from *HETE-2* data, about 12 XRFs should be added to the sample. If the redshift distributions of GRBs and XRFs are similar, the addition of about 12 XRFs should not change the shape of the redshift distribution very much. In addition, the best fits to the observed redshift distribution are the simulated bursts with large fluences, and

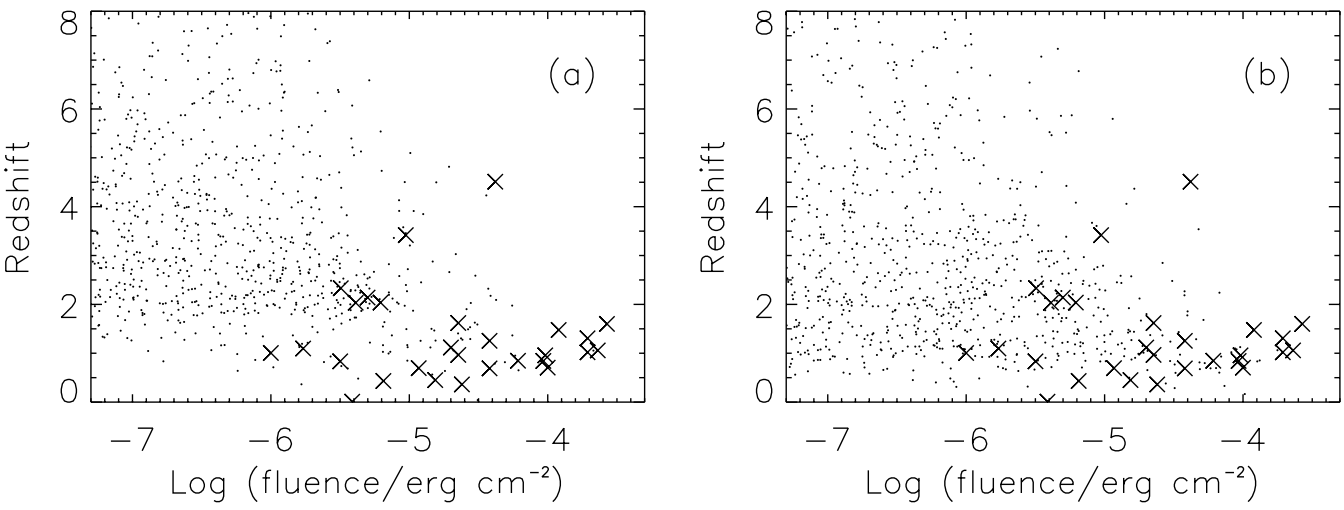

FIG. 2.—(*a*) Redshift vs. fluence plot for the simulated bursts (*dots*) and the observed bursts (*crosses*) from Bloom et al. (2003) with a $z_{\rm peak} = 2$ Rowan-Robinson star-forming rate. (*b*) Same as (*a*), but for $z_{\rm peak} = 1$.

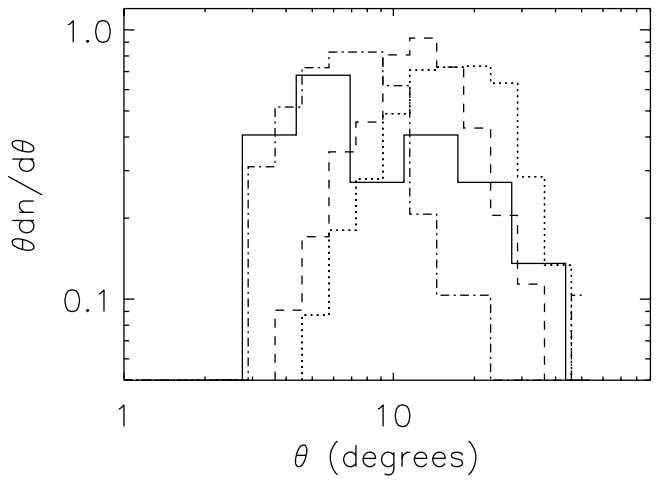

FIG. 3.—Normalized distributions of the observed jet angles (*solid line*) obtained from Bloom et al. (2003) and the simulated jet angles with detection thresholds of 5×10^{-8} (*dotted line*), 5×10^{-7} (*dashed line*), and 1×10^{-5} ergs cm^{-2} (*dash-dotted line*). The reason to choose a high fluence limit, such as 1×10^{-5} ergs cm^{-2}, is that only a small fraction of total bursts have their jet break angles measured. The median fluence of the 16 bursts with jet break angle measurements is 2.3×10^{-5} ergs cm^{-2} (Bloom et al. 2003), even higher than the highest fluence threshold we adopt.

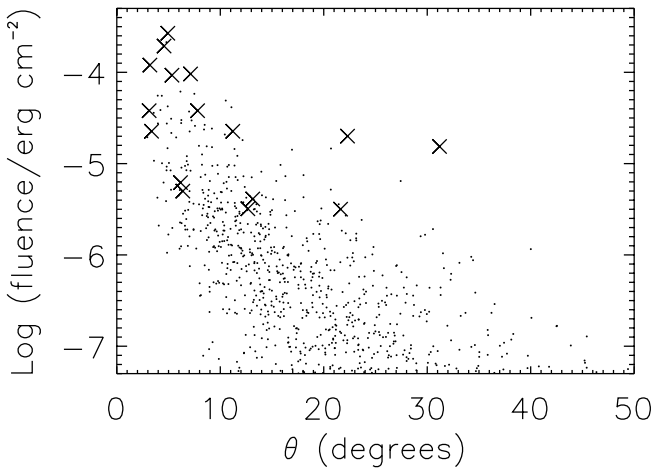

FIG. 4.—Fluence vs. jet break angle plot for the simulated bursts (*dots*) and the observed bursts (*crosses*) from Bloom et al. (2003) with a $z_{\rm peak} = 2$ Rowan-Robinson star-forming rate.

according to the $E^{\rm obs}_{\rm peak}$-fluence relation of the *HETE-2* bursts, these high-fluence bursts ($>1.0\times10^{-5}$ ergs cm^{-2}) should all be GRBs. Similar arguments also apply to the following simulations of the jet break angle distribution and the two-dimensional jet break angle versus redshift distribution.

3.2. *Jet Break Angle Distribution*

We plot the distribution of the jet break angle of the simulated bursts with different detection thresholds and the observed jet break angle distribution in Figure 3. The observed jet break angles are obtained from Bloom et al. (2003), and there are 16 bursts with jet break angle measurements. We exclude the bursts with upper or lower limit measurements on the jet break angles when comparing with the simulation results. The shape of the observed jet break angle distribution is sensitive to the bin size chosen because of the small sample size. However, the peak of the jet angle distribution can roughly be constrained at about 7°. In this simulation, we also apply different fluence filters to the simulated bursts to simulate the effect of the limited detector sensitivities. In particular, we adopt the fluence thresholds of 1.0×10^{-5}, 5.0×10^{-7}, and 5.0×10^{-8} ergs cm^{-2}. Figure 3 shows that the simulated jet break angle distribution is also sensitive to the detection threshold used in the simulation. The peak of the simulated distribution will move to larger angles when a lower threshold is selected. This is consistent with the result of Perna et al. (2003), who discovered this effect from the universal jet model. The simulated distribution with a fluence limit of 1.0×10^{-5} ergs cm^{-2} is consistent with the observed jet break angle distribution. Considering the difficulties in identifying the optical afterglows and in measuring the jet break angles, such a high threshold is a reasonable choice when comparing the simulation with the observations. The median fluence of the 16 bursts with jet break angle measurements is 2.3×10^{-5} ergs cm^{-2} (Bloom et al. 2003), even higher than the highest fluence limit we adopt. Only five of the 16 bursts have fluences lower than 1.0×10^{-5} ergs cm^{-2}, and the faintest one has a fluence of 3.17×10^{-6} ergs cm^{-2}. Considering that there are some bursts that are brighter than the fluence limit we adopt but whose jet break angles are still not measured, it is more reasonable to compare the median fluence, rather than the smallest fluence, of the 16 bursts. In Figure 4, we show the fluence versus jet break angle plot for the simulated bursts and the observed bursts (Bloom et al. 2003). Most of the observed bursts are in high-fluence regions. We also compare the jet break angle distribution with the predictions from the $z_{\rm peak} = 1$ Rowan-Robinson star-forming rate and reach similar results.

We reach a conclusion similar to that of Perna et al. (2003) that the predicted jet break angle distribution of structured jets is consistent with the currently observed sample distribution. While Perna et al. (2003) discussed the universal jets, our simulations are for Gaussian-like jets. We note that the detection threshold used in Perna et al. (2003) is the 90% efficiency peak flux threshold for BATSE, which is much more sensitive than the threshold we have adopted in the simulation that results in consistency between the data and the simulation. Since only a small fraction of bright GRBs have jet break angle measurements, it may be more appropriate to use a higher threshold than the BATSE detection threshold. When a higher threshold is selected, the θ_j distribution peak for the universal jet model should move to a smaller value comparing with the observed one. Liang et al. (2004b) also noticed this independently and also adopted a high threshold in their simulations.

3.3. *Redshift versus Jet Break Angle*

The jet break angle distribution discussed previously is a one-dimensional distribution, which includes bursts at all redshifts. As pointed out by Nakar et al. (2004), a more accurate test is to perform a two-dimensional (z-θ_j) distribution comparison between the data and the model prediction. It is possible that the two-dimensional distribution does not agree with the observations, while by integrating over redshift, the one-dimensional distribution agrees with the observations by chance.

In Figure 5 we plot the simulated data points with different fluence thresholds (same as those used in the one-dimensional plot) together with the 16 bursts with both redshift and jet break angle measured (Bloom et al. 2003). The density of the data points represents the probability density function (pdf) of this two-dimensional distribution. The plot shows that the pdf depends on the threshold of the detector. As the threshold goes higher, the peak of the pdf moves toward the region containing smaller jet break angles. This is consistent with the result from

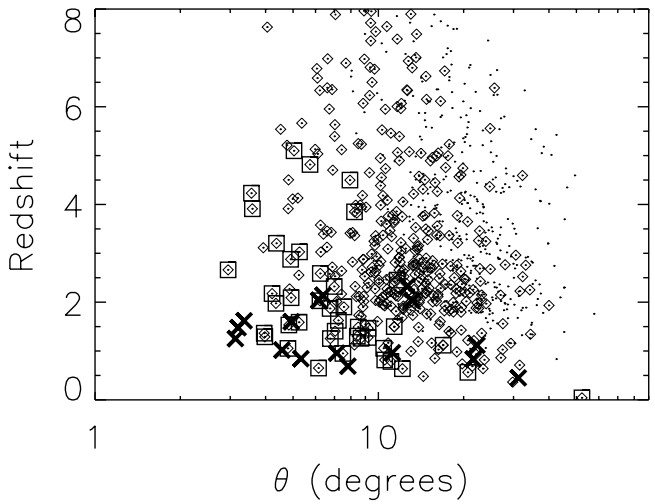

FIG. 5.—Redshift vs. jet angle plot for the observed burst sample (*crosses*) obtained from Bloom et al. (2003) and the simulated bursts with detection thresholds of 5×10^{-8} (*dots*), 5×10^{-7} (*diamonds*), and 1×10^{-5} ergs cm^{-2} (*squares*).

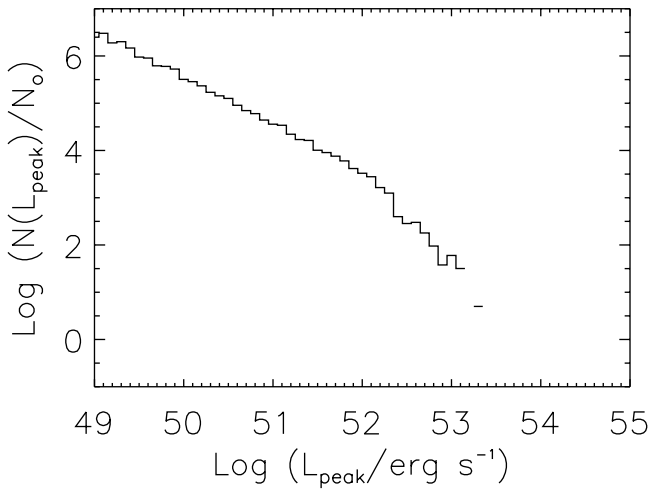

FIG. 6.—Luminosity function of GRBs with a quasi-universal Gaussian-like jet structure. The simulated luminosity function can be characterized by a broken power law, with the power-law indices of approximately -2 in the high-luminosity part ($L > 10^{52}$ ergs^{-1}) and approximately -1 in the low-luminosity part ($L < 10^{52}$ ergs^{-1}). This is consistent with that obtained from Schmidt (2001), except for the low-luminosity end below 10^{50} ergs^{-1}.

the one-dimensional analysis. In particular, the distribution of simulated bursts with the highest threshold is consistent with the observational distribution. Even when we limit the data points from a narrow redshift bin ($0.8 < z < 1.7$) that includes most of the observational data points, the simulated distribution and observational distribution is still consistent. Again, a high threshold is reasonable in this analysis, since the bursts with jet break angle measurements are much brighter on average than the ones in the whole sample of the detected bursts.

Nakar et al. (2004) argued that this two-dimensional distribution from the prediction of a universal jet does not agree with the observation, especially for the bursts within the redshift range of $0.8 < z < 1.7$. As we have shown previously (Lloyd-Ronning et al. 2004), the $E_{\rm iso}$-θ_j data already require that the model be quasi-universal, thus the inconsistency suggested by Nakar et al. (2004) is largely due to their adopting a nonvarying universal jet model. In particular, the sharp boundary of the region allowed by the universal model should smooth out if a quasi-universal model is considered (as shown in Fig. 5). Moreover, the detection threshold used in Nakar et al. (2004) is also the BASTE detection threshold, which is much more sensitive compared with the burst sample with jet break angle measurements. In addition, we adopted a Gaussian-like jet structure, while they stick to the power-law structure, which suffers other problems (e.g., numbers of XRFs with respect to GRBs and the $\log N-\log P$ distribution) as well.

3.4. *Luminosity Function*

We plot the luminosity function of the present quasi-universal Gaussian-like jet model in Figure 6. This luminosity function is an update of the result presented in Lloyd-Ronning et al. (2004). In Lloyd-Ronning et al. (2004) the total energy of the jet was taken as a constant rather than quasi-universal. When the total energy scatter is introduced, the simulated luminosity function does not show a bump at the break of the power-law index (cf. Figs. 9 and 10 in Lloyd-Ronning et al. 2004). In addition, we have performed a rigorous calculation of the total energy instead of using the approximation for small angles. At large angles, this difference is more than a factor of 2.

The simulated luminosity function can be characterized by a broken power law, with a power-law index of approximately -2 at the high-luminosity end ($L > 10^{52}$ ergs^{-1}) and an index of approximately -1 for low luminosities ($L < 10^{52}$ ergs^{-1}). The simulated luminosity function is consistent with previous simulations of Gaussian jets performed in Lloyd-Ronning et al. (2004), except that there is no big bump at the break of the power index this time. Currently, the GRB luminosity function is not directly determined from the observations, since the sample of bursts with redshift measurement is too small. Nonetheless, there are several attempts to constrain the luminosity function through various approaches (e.g., Schmidt 2001; Norris 2002; Lloyd-Ronning et al. 2002; Stern et al. 2002; Firmani et al. 2004). In general, many of these studies found a break of the luminosity function, with the power index steeper in the high-luminosity range and flatter in the low-luminosity range (see detailed discussions in Lloyd-Ronning et al. [2004] and references therein). This is consistent with the simulated luminosity function. In particular, the shape of the simulated luminosity function in this paper is very similar to that obtained from Schmidt (2001), except for the low-luminosity end below 10^{50} ergs^{-1}, for which the luminosity function from Schmidt (2001) turns over. This luminosity function obtained from Schmidt (2001) can fit the BASTE $\log N-\log P$ quite well, assuming a certain star-forming rate (Schmidt 2003).

3.5. $\log N-\log P$ *Distribution*

We use the $\log N-\log P$ plot as a final test to the jet structure used in this paper. The $\log N-\log P$ plot has been used to constrain the jet opening angle distribution for the uniform jet and the star-forming rate in previous studies (Lin et al. 2004; Guetta et al. 2005b). In particular, Guetta et al. (2005b) pointed out that the $\log N-\log P$ distribution predicted by the universal jet model overpredicts bursts with faint flux. This inconsistency is another manifestation of the problem of overproducing XRFs in the universal jet model (Lamb et al. 2005). Since the quasi-universal Gaussian jet model can overcome the latter difficulty, it is natural to expect that it can solve the former problem as well.

We use the bursts from the offline reanalyzed BATSE catalog (Kommers et al. 2000) including both triggered and untriggered

bursts. The catalog includes a total of 2167 bursts, of which 1393 are triggered bursts and 874 are untriggered bursts. The bursts selected in this catalog are all long GRBs, which are directly related to our model. In order to estimate the simulated peak photon flux, we assume a Band function (Band et al. 1993) for the simulated bursts and adopt the low- and high-energy photon indices as $\alpha = -1$ and $\beta = -2$. As our simulation stems from the data provided by Bloom et al. (2003) for which the isotropic energy is given in the 20–2000 keV band rest frame, we need to take into account the difference between the bandpass of BATSE and that used in Bloom et al. (2003). The fluence that we obtained from equation (15) should be

$$F = \int_{20/(1+z)\ \mathrm{keV}}^{2000/(1+z)\ \mathrm{keV}} EN(E)\,dE. \tag{20}$$

The photon fluence in the BATSE band (50–300 keV) reads

$$F^{\mathrm{ph}}_{\mathrm{BATSE}} = \int_{50\ \mathrm{keV}}^{300\ \mathrm{keV}} N(E)\,dE. \tag{21}$$

We can then calculate the photon fluence in the BATSE band using the energy fluence, i.e.,

$$F^{\mathrm{ph}}_{\mathrm{BATSE}} = \frac{F\int_{50\ \mathrm{keV}}^{300\ \mathrm{keV}} N(E)\,dE}{\int_{20/(1+z)\ \mathrm{keV}}^{2000/(1+z)\ \mathrm{keV}} EN(E)\,dE}. \tag{22}$$

The ratio between the two integrals in equation (22) only depends on the value of E_p (which is simulated in the code) when both α and β are assigned to their typical values.[5] Essentially, we use the energy fluence to determine the normalization of the Band function and calculate the photon fluence with the determined Band function. Finally, the peak photon flux can be obtained by dividing $F^{\mathrm{ph}}_{\mathrm{BATSE}}$ by the conversion timescale T defined in equation (16), i.e.,

$$f^{\mathrm{ph}}_{\mathrm{BATSE}} = \frac{F^{\mathrm{ph}}_{\mathrm{BATSE}}}{T(1+z)}. \tag{23}$$

We do not perform a fluence or energy truncation for the $\log N - \log P$ analysis (unlike in the previous sections). The BATSE sample is much more homogeneous and is free of most of the selection effects encountered for the other samples we have discussed (the sample with redshift or jet angle information). The simulated sample is naturally truncated with the offline detection threshold in peak photon flux (Kommers et al. 2000), i.e., 0.18 photons cm^{-2} s^{-1}. This is lower than the BATSE onboard detection threshold, 0.3 photons cm^{-2} s^{-1}. This peak photon flux truncation is adopted when we compare the simulated $\log N - \log P$ distribution with the observation through the Kolmogorov-Smirnov (K-S) test. Guided by the K-S test, we fit the simulated $\log N - \log P$ distribution to the observed distribution with a normalization parameter so that the simulated $\log N - \log P$ plot can be shifted vertically. The normalization reflects the difference between the number of the simulated bursts and the number of the true bursts in the BATSE sample. After the fitting, the simulated bursts fit very well with the observed $\log N - \log P$ plot. The $\log N - \log P$ distributions for the simulated bursts after the fitting and the bursts from BATSE catalog are shown in Figure 7. We perform a K-S test to the two cumulative distributions after the peak photon flux truncation at 0.18 photons cm^{-2} s^{-1} and a K-S chance probability of 11% is obtained, which implies that the simulated $\log N - \log P$ distribution cannot be rejected through the K-S test.

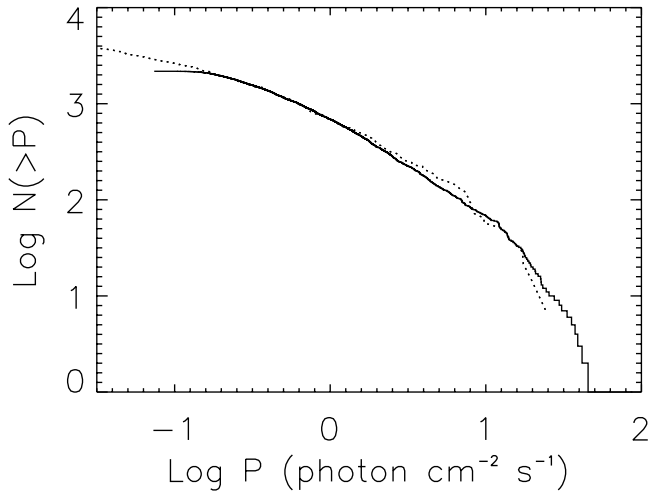

FIG. 7.—Plots of $\log N(>P) - \log P$ for the BATSE bursts (*solid histogram*; from Kommers et al. 2000) and the simulated bursts from the quasi-universal Gaussian-like model (*dotted line*). The universal jet fails to reproduce the $\log N(>P) - \log P$ distribution (Guetta et al. 2005b), as it predicts almost a power law $\log N(>P) - \log P$ distribution that unavoidably overpredicts bursts at the low-flux end. The simulation result from the quasi-universal Gaussian jet fits well with the BATSE $\log N(>P) - \log P$ distribution.

We also test the model with the $z_{\mathrm{peak}} = 1$ Rowan-Robinson star-forming rate and similar results are obtained. This result suggests that the observed BATSE $\log N - \log P$ distribution can be reproduced with this quasi-universal Gaussian structured jet model. We also compare the BATSE catalog from Kommers et al. (2000) with the GUSBAD catalog from Schmidt (2004), and the $\log N - \log P$ distributions obtained from the two catalog are generally consistent.

The simulated $\log N - \log P$ plot can generally reproduce the turnover behavior at the faint end, but it still deviates from the BATSE data at the lowest peak photon flux of the distribution. This does not affect the main result, because this deviation occurs at regions where the peak photon flux is below the limit of the BATSE offline search sensitivity so that a significant part of the burst could be missed. In addition, at the low-flux region the distribution is sensitive to the detection threshold adopted. We plot the simulated distribution extending down to a lower peak photon flux limit than BATSE as a prediction for future observations. In the simulation we did not perform any luminosity or E_{peak} truncation so that XRFs are also included in the simulated samples for this test. It is unclear if most XRFs have been detected with BATSE. Since a Band function (Band et al. 1993) has a typical upper photon spectral index $\beta \sim -2$ for GRBs, XRFs should be detected as faint GRBs as well if their high-energy photon spectral indices have a similar value. In addition, we also test the case by excluding the simulated burst with lower observed peak energies (e.g., those with $E^{\mathrm{obs}}_{\mathrm{peak}} < 10$ keV), and the resulting $\log N - \log P$ plot is still consistent with the data. The reason is that XRFs mainly contribute to the faintest population of the distribution.

We note that the simulated $\log N - \log P$ plot is also sightly different from the observed distribution at high photon fluxes.

[5] We have also tested the cases when α and β deviate from the nominal values. The results essentially remain unchanged.

However, the difference is not significant, because the number difference between the simulated and observed bursts is small. The difference could result from small-number statistical effects. This could be tested by increasing the number of simulated bursts. It may also indicate that the jet structure is closer to a power-law structure at small angles.

Guetta et al. (2005b) fitted the predicted $\log N - \log P$ distribution from the universal jet model and compared it with the observations. The total bursts (595) used in Guetta et al. (2005b) is smaller than the burst sample (2167 in total) used in this paper. However, even with a small sample, Guetta et al. (2005b) concluded that the universal jet model can be rejected from the $\log N - \log P$ distribution. With a quasi-universal Gaussian-like jet model, the observed $\log N - \log P$ distribution can be fitted quite well from the simulations performed in this paper, especially in the range of $-0.7 < \log P$ (photons cm^{-2} s^{-1}) < 1, for which the $\log N - \log P$ distribution is constrained most accurately. The major difference between a power-law jet and a Gaussian jet is at large angles. The exponential drop of the jet energy at large angles in the Gaussian model is the key to reducing the correct number of faint bursts in the BATSE sample. The problem faced by the universal jet model in the $\log N - \log P$ distribution test is avoided with the quasi-universal Gaussian jet model.

Recently, Guetta et al. (2005a) claimed that a power-law jet truncated at large angles can also reproduce the BATSE $\log N - \log P$ distribution. This is consistent with our argument raised in this paper. Considering that a Gaussian jet invokes a natural exponential drop-off at large angles while a reasonable power-law jet model has to invoke both a small angle and a large angle artificial break, we deem that the quasi-universal Gaussian jet model is a more elegant one. We note that the $\log N - \log P$ distribution is more sensitive to the jet structure than to the GRB distribution with redshift. It is therefore a powerful tool for pinning down the correct jet structure.

4. CONCLUSION AND DISCUSSION

We perform Monte Carlo simulations of a quasi-universal Gaussian-like structured jet and compare the simulation results with a wide spectrum of current observations. The simulation results for the Gaussian-like jet used in this paper are generally consistent with various observational constraints, including the burst redshift distribution, jet break angle distribution, two-dimensional distribution of redshift and jet break angle, luminosity function, and $\log N - \log P$ distribution. This result is complementary to the previous simulation results (Zhang et al. 2004) that showed that the number ratios among GRBs, XRGRBs, and XRFs, the observed jet break angle versus isotropic energy relation, and the observed peak energy versus fluence relation are consistent with predictions from this jet model.

Although the samples of different burst properties used for some tests in this paper are small such that very detailed constraints on the jet structure cannot be achieved, the global test performed on the quasi-universal Gaussian jet model (including this paper and the previous work, Zhang et al. 2004) at least suggests the following two major conclusions. First, in order to unify GRBs and XRFs through viewing angle effects such that GRBs are viewed from small observing angles and XRFs are viewed from large observing angles, the jet energy at large angles must drop exponentially. This comes from two constraints: the $\log N - \log P$ distribution and the number ratios among GRBs, XRGRBs, and XRFs. This requirement is consistent with the Gaussian jet model. The power-law jet structure cannot extend to large angles. Otherwise, it will overproduce the number of XRFs and low-flux bursts in the $\log N - \log P$ distribution. Second, "quasi-universal" should also be an essential ingredient for the jet models, as it is unrealistic to assume that all the GRB progenitors, their environments, and other properties are exactly the same. The quasi-universal nature is crucial to fit the $E_{\rm iso}$-θ_j relation, and it could produce the luminosity function power-law index break that was implicated in many studies. A quasi-universal Gaussian-like jet is suitable for both constraints. We also note that many burst property distributions are sensitive to the detection threshold selected, and a suitable threshold for the current sample should be selected carefully when comparing the model predictions with the observations.

Currently, the detailed jet structure at small angles is not well constrained. The slope may be steeper than that in the Gaussian model. It is possible that the Gaussian jet slightly underpredicts bright bursts as indicated from the $E_{\rm peak}^{\rm obs}$-fluence plot and the $E_{\rm iso}$-θ_j plot in Zhang et al. (2004). Such a deficit, however, could be well due to selection effects, since the brightest bursts are those easiest to detect and to localize. If the deficit is real, it may be accounted for through possible evolution of the GRB luminosity function, which was suggested by recent studies (Lloyd-Ronning et al. 2002; Wei & Gao 2003; Yonetoku et al. 2004; Graziani et al. 2004). It may also be understood in terms of the two-component jet picture (Berger et al. 2003; Huang et al. 2004; Liang & Dai 2004), in which a bright core component contributes to more bright bursts. These issues can be tested thoroughly with a larger, homogeneous sample of bursts accumulated.

In the *Swift* era, the sample of GRBs with redshift and jet break angle measurements is anticipated to be much larger than the current sample. In addition, these bursts will form a homogeneous sample that is most suitable to apply statistical analyses on various burst properties. We anticipate most of the GRB relations used in this paper and Zhang et al. (2004) will be constrained more accurately, except for the $\log N - \log P$ distribution. With refined Monte Carlo simulations of this and other models, the details of GRB jet structure can be pinned down more precisely through statistical analyses of the observed burst properties and the model predictions.

We thank Nicole Lloyd-Ronning and Peter Mészáros for stimulative collaborations, Don Lamb, Rosalba Perna, Dale Frail, and S. N. Zhang for extensive discussion on GRB jets, Maarten Schmidt, E. W. Liang, Z. G. Dai, and Dafne Guetta for helpful comments, and the anonymous referee for helpful suggestions. We also acknowledge Jefferson M. Kommers for providing the BATSE catalog of triggered and untriggered burst data. This work is supported by Swift GI program (Cycle 1) (for both authors), a NASA grant NAS8-01128 (for X. D.), and a NASA LTSA program NNG04GD51G (for B. Z.).

REFERENCES

Amati, L., et al. 2002, A&A, 390, 81
Band, D., et al. 1993, ApJ, 413, 281
Berger, E., et al. 2003, Nature, 426, 154
Bloom, J. S., Frail, D. A., & Kulkarni, S. R. 2003, ApJ, 594, 674
Firmani, C., Avila-Reese, V., Ghisellini, G., & Tutukov, A. V. 2004, ApJ, 611, 1033
Frail, D. A., et al. 2001, ApJ, 562, L55
Graziani, C., et al. 2004, in AIP Conf. Proc. 727, Thirty Years of Discovery: 2003 Gamma-Ray Burst Symp. (New York: AIP), 42

Guetta, D., Granot, J., & Begelman, M. C. 2005a, ApJ, in press (astro-ph/0407063)
Guetta, D., Piran, T., & Waxman, E. 2005b, ApJ, 619, 412
Harrison, F. A., et al. 1999, ApJ, 523, L121
Heise, J. 2003, AIP Conf. Proc. 662, Gamma-Ray Burst and Afterglow Astronomy 2001: A Workshop Celebrating the First Year of the *HETE* Mission (New York: AIP), 229
Huang, Y. F., Wu, X. F., Dai, Z. G., Ma, H. T., & Lu, T. 2004, ApJ, 605, 300
Kippen, M., et al. 2003, AIP Conf. Proc. 662, Gamma-Ray Burst and Afterglow Astronomy 2001: A Workshop Celebrating the First Year of the *HETE* Mission (New York: AIP), 244
Kommers, J. M., et al. 2000, ApJ, 533, 696
Kulkarni, S. R., et al. 1999, Nature, 398, 389
Kumar, P., & Granot, J. 2003, ApJ, 591, 1075
Lamb, D. Q., Donaghy, T. Q., & Graziani, C. 2005, ApJ, 620, 355
Liang, E. W., & Dai, Z. G. 2004, ApJ, 608, L9
Liang, E. W., Dai, Z. G., & Wu, X. F. 2004a, ApJ, 606, L29
Liang, E. W., Wu, X. F., & Dai, Z. G. 2004b, MNRAS, 354, 81
Lin, J. R., Zhang, S. N., & Li, T. P. 2004, ApJ, 605, 819
Lloyd, N. M., Petrosian, V., & Mallozzi, R. S. 2000, ApJ, 534, 227
Lloyd-Ronning, N. M., Dai, X., & Zhang, B. 2004, ApJ, 601, 371
Lloyd-Ronning, N. M., Fryer, C. L., & Ramirez-Ruiz, E. 2002, ApJ, 574, 554
Nakar, E., Granot, J., & Guetta, D. 2004, ApJ, 606, L37
Norris, J. P. 2002, ApJ, 579, 386
Perna, R., Sari, R., & Frail, D. 2003, ApJ, 594, 379
Rhoads, J. E. 1999, ApJ, 525, 737
Rossi, E., Lazzati, D., & Rees, M. J. 2002, MNRAS, 332, 945
Rossi, E. M., Lazzati, D., Salmonson, J. D., & Ghisellini, G. 2004, MNRAS, 354, 86
Rowan-Robinson, M. 1999, Ap&SS, 266, 291
Sakamoto, T., et al. 2004, ApJ, 602, 875
Schmidt, M. 2001, ApJ, 552, 36
———. 2003, preprint (astro-ph/0301277)
———. 2004, ApJ, 616, 1072
Stern, B. E., Tikhomirova, Y., & Svensson, R. 2002, ApJ, 573, 75
Wei, D. M., & Gao, W. H. 2003, MNRAS, 345, 743
Yamazaki, R., Ioka, K., & Nakamura, T. 2003, ApJ, 593, 941
Yonetoku, D., Murakami, T., Nakamura, T., Yamazaki, R., Inoue, A. K., & Ioka, K. 2004, ApJ, 609, 935
Zhang, B., Dai, X., Lloyd-Ronning, N. M., & Mészáros, P. 2004, ApJ, 601, L119
Zhang, B., & Mészáros, P. 2002a, ApJ, 571, 876
———. 2002b, ApJ, 581, 1236